Integration of a Low-Cost Three-Axis Sensor for Robot Force Control

Shuyang Chen[1], Jianren Wang[2] and Peter Kazanzides[2]

Abstract—Many robot systems incorporate six-axis force/torque sensors to enable compliant interaction with the environment, even when a lower-cost three-axis sensor may be sufficient. One challenge is that a three-axis sensor may measure a coupling of the applied forces and torques; these can be decoupled with an appropriate calibration and with assumed knowledge of the location of the applied force. In this paper, we develop the method and open source software to calibrate a commercially-available three-axis sensor and verify its performance in static tests with known weights and in dynamic tests by comparison to an accurate six-axis sensor. Mean errors in static tests are less than 5% and experiments demonstrate that the sensor can be used to control the contact force applied by a robot-held ultrasound probe.

Fig. 1: CAD drawings of the OptoForce sensor [5]

I. INTRODUCTION

Multi-axis force and torque sensors are commonly used in robot systems due to their ability to measure environment interactions in multiple dimensions. Their working principle is to measure small deflections due to the applied force and torque and to convert these measurements into the estimated force and torque, typically using a calibration matrix. Commercially-available six-axis force/torque sensors, however, are relatively expensive (typically on the order of $5,000 US) and easy to damage due to force overloads. At the same time, there are many cases where a six-axis force sensor is used even though fewer axes, or degrees of freedom (DOF), would suffice. For example, force sensors are often used for cooperative control, where a human can "hand guide" a robot by grabbing the end-effector and applying forces, which are sensed by the force sensor and cause the robot to move in the desired direction. While simultaneous position and orientation guidance requires a 6-DOF force sensor, it has been observed since at least the early 1990s that it is often easier to decouple position and orientation guidance [1], in which case a 3-DOF sensor would be sufficient. Also, in cases where a robot is probing a surface, it is often sufficient to consider only the (3 DOF) force vector.

This work was motivated by the development of two generations of cooperatively-controlled robots for providing ultrasound guidance during patient setup for radiotherapy [2], [3]; the first generation system was also used to test acoustic radiation force (ARF) imaging [4]. In all of these systems, a six-axis force/torque sensor was mounted at the robot end-effector and used to provide cooperative control and/or to control the contact force of the ultrasound probe. We realized, however, that a three-axis sensor would have been sufficient and would
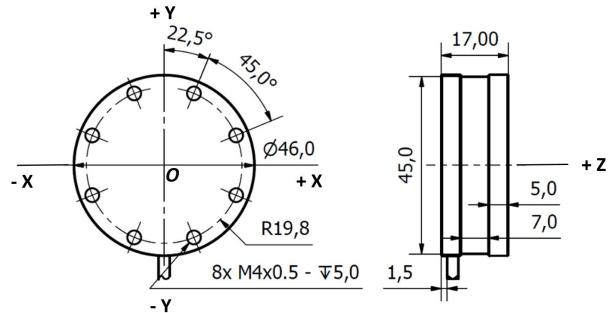
have reduced the system cost. One challenge is that a three-axis sensor typically measures a combination of the applied forces and torques. But, it is possible to decouple forces and torques if we assume a known single point of contact. While this is a strong assumption, it may be reasonable for cases such as cooperative control (assuming the robot contains a handle for the operator to grasp) or for probing with a tool.

We therefore considered a low-cost three-axis sensor based on optical principles from OptoForce Ltd. (Budapest, Hungary). While many OptoForce 3-DOF sensors have a rounded dome and are intended for applications such as fingertip force sensing, the company also markets flat-top, three-axis sensors, such as the OMD-45-FE-1000N shown in Fig. 1 (this specific model is no longer available, but similar flat-top models are available).

This paper describes the software and calibration methods that enable integration of a low-cost three-axis sensor for applications such as cooperative control and surface probing. Section II presents the calibration method, which obtains a calibration matrix that converts the three sensor measurements into three forces, assuming a known moment arm. Results of the static and dynamic tests of the sensor performance, as well as results of robot force control, are given in Section III. Our goal is to provide a practical solution, disseminated through open source software, that can enable others to utilize low-cost force sensors in their robotic research.

II. METHODS

A. Software Interface

We created an open source software component compatible with the Surgical Assistant Workstation (SAW) package [6], which is based on the *cisst* libraries [7]. This component is available at https://github.com/jhu-saw/sawOptoforceSensor. It is implemented in C++ and consists of a single thread that receives data streamed from the OptoForce sensor and caches it locally in a data structure (i.e., the *cisst* State Table). Sensor

[1]Department of Mechanical Engineering, Rensselaer Polytechnic Institute, Troy, NY 12180, USA chens26@rpi.edu
[2]Department of Computer Science, The Johns Hopkins University, Baltimore, MD 21218, USA pkaz@jhu.edu

IEEE computer society

parameters, such as the scale factor, filter cutoff frequency, communication rate (100 Hz by default, but configurable up to 1000 Hz), and the calibration matrix described below, are specified via a JavaScript Object Notation (JSON) configuration file. A Robot Operating System (ROS) [8] interface, via a *cisst-to-ROS* bridge, facilitates integration with other devices.

B. Calibration Method

We adopt a conventional least-squares approach [9], [10], [11], with a small modification to incorporate the assumed moment arm. We chose this approach because it would enable a more intuitive understanding of possible nonlinearities, for example, due to the fact that forces are measured based on deformation of an underlying rubber dome structure.

We use the following linear model to convert the coupled force and resulting moment vector M into the sensor reading vector S:

$$S = AM \qquad \text{or} \qquad S^T = M^T A^T \qquad (1)$$

where $S \in R^3$ is the vector of sensor readings (S_x, S_y, S_z), A is a 3×6 constant calibration matrix that produces the mapping and is a characteristic of the mechanical structure of the sensor, and $M \in R^6$ is the vector of coupled applied force and moment. The moment is determined by the positional information of the applied force relative to the coordinate frame of the sensor shown in Fig. 1.

We collect N measurements in three Cartesian directions corresponding to forces applied (2 N, 3 N, 5 N, 7 N, 8 N in our case) at different locations, using the simple platform shown in Fig. 2. Then, we build an over-determined linear system of equations to solve A. We added an application program to the *sawOptoforceSensor* repository that integrates data acquisition, data store and matrix calculation. The choice of N was experimentally determined to be within the range of $25 \sim 50$, which will generate a repeatable and relatively accurate calibration matrix. For our subsequent experiments, we chose $N = 30$.

(a) Weights applied in x or y direction   (b) Weights applied in z direction
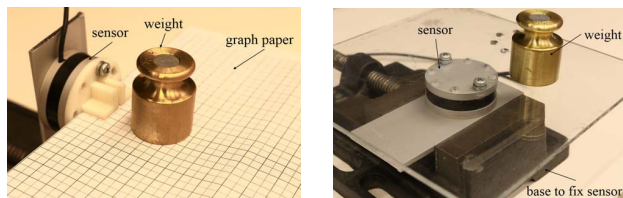
Fig. 2: Experimental setup for sensor calibration

III. EXPERIMENTAL EVALUATION

We performed static and dynamic tests to evaluate the performance of the calibrated OptoForce sensor; dynamic testing included robot force control.
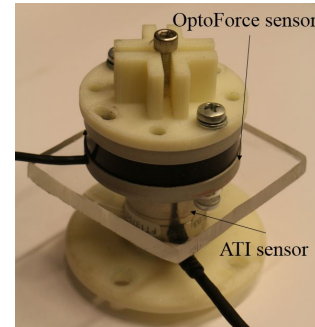
Fig. 3: Setup to compare OptoForce with ATI Nano25

A. Static Tests

Using the same setup as for calibration, we applied 10 different weights (1 N, 2 N,..., 10 N) to different locations in three Cartesian directions and calculated the nominal forces. For each weight, we repeated the measurement three times. Table I displays the comparison between the raw applied weights and the corresponding calculated forces in specific locations for the x, y and z directions, respectively (all the locations are relative to the coordinate frame of the OptoForce sensor with units of millimeters, as shown in Fig. 1).

The data in Table I show that the calibration matrix can produce reliable results for static applied weights, with less than 5% relative errors in the direction of the applied weights. Also, there are negligible force readings (no more than 7.7% relative to the applied weights) in other directions, which indicates that the calibration matrix has effectively decoupled the axes.

We conducted static tests with another OMD-45-FE-1000N sensor to study the consistency of the calculated calibration matrix between different force sensors of the same type. The results, shown in Table II, indicate that a single calibration matrix might suffice for all force sensors of this type, though further tests are required to verify this hypothesis.

B. Dynamic Tests

We performed dynamic tests by comparing the calibrated OptoForce sensor to a Nano25 six-axis force sensor (ATI Industrial Automation, Apex, NC), interfaced via a NI-DAQ board (National Instruments, Austin, TX), that provided the ground truth. We rigidly fixed the two sensors and carefully aligned their Cartesian axes, as shown in Fig. 3. We held the upper end of the ATI sensor and manually pushed the OptoForce sensor to make it contact with a surface at a fixed location and orientation, applying arbitrary forces (mostly in the z direction) for 30 seconds while sampling both sensor readings at 10 Hz. We did not apply software filtering to either the ATI or OptoForce sensor readings. Nevertheless, it is possible that some filtering was applied in the lower-level hardware. Figure 4 compares both sensor outputs for a test performed at location (11.2, -15.5, -8.2) mm. The root-mean-square errors (RMSE) for the x, y, and z components of the force vector are 0.22 N, 0.30 N and 0.82 N, respectively, and the RMSE for the force magnitude (norm) is 0.78 N. These results show that the calibrated OptoForce sensor reading tracks

TABLE I: Results of static tests for applied weights from 1 N to 10 N, at different position offsets, along x, y, and z directions. Showing mean calibrated sensor output, standard deviation, and percent error (percentage of applied weight). Bold value indicates corresponding component in direction of applied weight.

Applied Weight (N)	1	2	3	4	5	6	7	8	9	10
Weights applied in -x direction at (1.58, 0, -53.93) mm										
Mean Sensor Output (N)	**-0.970**, 0, 0.027	**-1.960**, 0, 0.113	**-2.940**, 0, 0.147	**-3.943**, 0, 0.193	**-4.993**, 0, 0.240	**-5.993**, 0, 0.370	**-6.993**, 0, 0.410	**-7.953**, 0, 0.413	**-8.993**, 0, 0.500	**-9.983**, 0, 0.557
Standard Deviation	**0.040**, 0, 0.038	**0.046**, 0, 0.025	**0.026**, 0, 0.032	**0.061**, 0, 0.042	**0.078**, 0, 0.070	**0.038**, 0, 0.061	**0.040**, 0, 0.050	**0.050**, 0, 0.081	**0.049**, 0, 0.046	**0.071**, 0, 0.061
Error (% of Applied Weight)	**3.0**, 0, 2.7	**2.0**, 0, 5.7	**2.0**, 0, 4.9	**1.4**, 0, 4.8	**0.1**, 0, 4.8	**0.1**, 0, 6.2	**0.1**, 0, 5.9	**0.6**, 0, 5.2	**0.1**, 0, 5.6	**0.2**, 0, 5.6
Weights applied in -y direction at (0, 1.58, -53.93) mm										
Mean Sensor Output (N)	0, **-0.960**, 0.077	0, **-1.933**, 0.120	0, **-2.963**, 0.093	0, **-3.987**, 0.160	0, **-4.977**, 0.320	0, **-5.973**, 0.443	0, **-6.977**, 0.393	0, **-8.037**, 0.407	0, **-9.053**, 0.400	0, **-10.077**, 0.450
Standard Deviation	0, **0.044**, 0.067	0, **0.025**, 0.036	0, **0.040**, 0.060	0, **0.085**, 0.056	0, **0.032**, 0.044	0, **0.035**, 0.057	0, **0.035**, 0.025	0, **0.059**, 0.035	0, **0.021**, 0.036	0, **0.042**, 0.066
Error (% of Applied Weight)	0, **4.0**, 7.7	0, **3.4**, 6.0	0, **1.2**, 3.1	0, **0.3**, 4	0, **0.5**, 6.4	0, **0.5**, 7.4	0, **0.3**, 5.6	0, **0.5**, 5.1	0, **0.6**, 4.4	0, **0.8**, 4.5
Weights applied in +z direction at (0, 0, 0) mm										
Mean Sensor Output (N)	0, 0, **1.030**	0, 0, **1.983**	0, 0, **3.013**	0, 0, **4.010**	0, 0, **4.980**	0, 0, **5.970**	0, 0, **7.000**	0, 0, **8.010**	0, 0, **8.967**	0, 0, **10.027**
Standard Deviation	0, 0, **0.089**	0, 0, **0.080**	0, 0, **0.045**	0, 0, **0.075**	0, 0, **0.036**	0, 0, **0.085**	0, 0, **0.082**	0, 0, **0.046**	0, 0, **0.065**	0, 0, **0.116**
Error (% of Applied Weight)	0, 0, **3.0**	0, 0, **0.9**	0, 0, **0.4**	0, 0, **0.3**	0, 0, **0.4**	0, 0, **0.5**	0, 0, **0**	0, 0, **0.1**	0, 0, **0.4**	0, 0, **0.3**

TABLE II: Results of static tests with another OMD-45-FE-1000N sensor for applied weights from 2 N to 5 N, presented in same format as Table I.

Applied Weight (N)	2	3	4	5
Weights applied in -x direction at (13.64, 13.96, -39.21) mm				
Mean Sensor Output (N)	**-1.947**, 0, 0.200	**-3.003**, 0, 0.167	**-3.987**, 0, 0.123	**-5.017**, 0, 0.143
Standard Deviation	**0.025**, 0, 0.030	**0.067**, 0, 0.006	**0.057**, 0, 0.040	**0.076**, 0, 0.023
Error (% of Applied Weight)	**2.7**, 0, 10	**0.1**, 0, 5.6	**0.3**, 0, 3.1	**0.3**, 0, 2.9
Weights applied in +y direction at (11.16, 20.12, -39.21) mm				
Mean Sensor Output (N)	0, **2.017**, 0.157	0, **3.050**, 0.150	0, **4.020**, 0.117	0, **5.043**, 0.137
Standard Deviation	0, **0.035**, 0.023	0, **0.020**, 0.035	0, **0.046**, 0.050	0, **0.031**, 0.058
Error (% of Applied Weight)	0, **0.9**, 7.9	0, **1.7**, 5	0, **0.5**, 2.9	0, **0.9**, 2.7
Weights applied in +z direction at (0, 0, -6.14) mm				
Mean Sensor Output (N)	0, 0, **2.010**	0, 0, **3.007**	0, 0, **4.013**	0, 0, **4.987**
Standard Deviation	0, 0, **0.020**	0, 0, **0.049**	0, 0, **0.057**	0, 0, **0.031**
Error (% of Applied Weight)	0, 0, **0.5**	0, 0, **0.2**	0, 0, **0.3**	0, 0, **0.3**
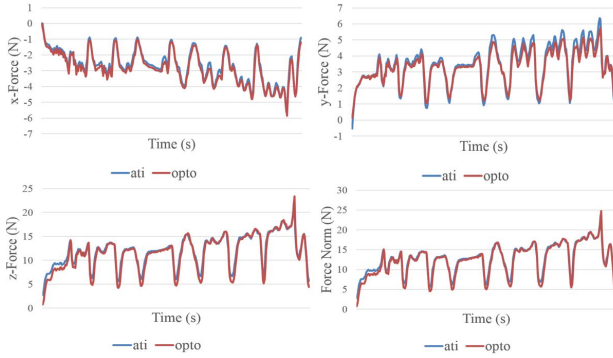
Fig. 4: Result of one dynamic test. The location of the applied forces is (11.2, -15.5, -8.2) mm

the ATI force sensor reading under dynamic conditions, with RMSE less than 1 N.

C. Robot Force Control

We demonstrate use of the calibrated three-axis sensor for force control with a UR3 robot (Universal Robots, Odense, Denmark). Although the UR series of robots are collaborative robots and offer a *free drive* mode, in prior research we determined that a wrist-mounted force sensor was necessary to provide precise "hands on" control of a tool-mounted ultrasound probe [2]. In that work, we provided cooperative control by mounting an ATI 6-axis force sensor on the wrist of a UR5 robot and connecting it to a PC that computed desired joint velocities based on the measured force. For the experiments

reported in this paper, we mounted the OptoForce sensor on the tool flange of the UR3 robot and connected a passive arm and ultrasound (US) probe to the sensor. The Optoforce filter cutoff frequency was set to 15 Hz. We used the same force control algorithm as before [4], which consists of a PID controller on the force error that produces a desired velocity (i.e., admittance control); the PID parameters are: $k_p = 0.8$, $k_d = 0.1$, and $k_i = 0.005$. We connected to the UR3 robot via its real-time script interface (TCP/IP socket to port 30003) using the open source *mtsUniversalRobotScriptRT* SAW component, available at https://github.com/jhu-saw/sawUniversalRobot. We mounted an ATI six-axis force/torque sensor in the environment to provide the ground-truth force measurements.

To support ultrasound guidance for radiotherapy [2], it is necessary to provide force control along the US probe axis. Thus, we introduce two optical markers and a Polaris optical tracker (Northern Digital, Waterloo, Canada), as shown in Fig. 5. The optical tracking system measures the pose of the marker on the US probe with respect to the marker attached to the robot base. A number of methods can be used to determine: (1) the fixed transformation between the US probe marker and the US probe tip, and (2) the fixed transformation between the robot base marker and the robot world coordinate system. In this study, we measured the transformations using the optical tracking system and a tracked tool, but it could alternatively be solved as a standard hand/eye calibration problem [12]. Once these transformations are determined, the pose of the US probe tip can be reported with respect to the robot world coordinate system or the wrist-mounted force sensor.

We conducted force control experiments with three different desired forces: 5 N, 10 N and 20 N. The location of the US probe tip with respect to the sensor frame was (46, 103, -142) mm, obtained from the optical tracking system measurement. We then controlled the UR3 so that the US probe tip contacted the ATI sensor for 30 seconds, while sampling both sensor readings, in the z axis, at 20 Hz. The results are plotted in Fig. 6. The RMSE of the OptoForce sensor with respect to the ATI sensor was 0.232 N, 0.515 N, and 0.968 N, when the desired force was specified as 5 N, 10 N, and 20 N, respectively. Dividing RMSE by the desired force indicates that the calibrated OptoForce sensor is within 5% of the ATI sensor for the dynamic condition of force control.
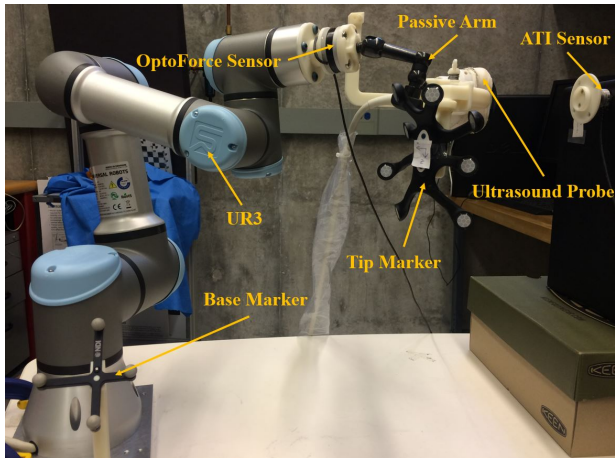
Fig. 5: Force control experiment setup, with US probe pose measured by optical tracking system
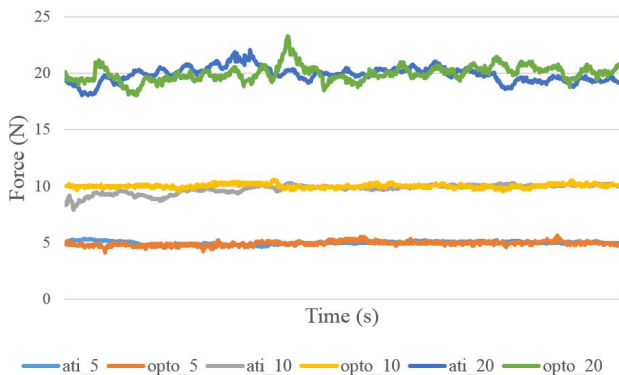
Fig. 6: Forces measured by Optoforce and ATI sensors during force control along US probe axis

IV. DISCUSSION AND CONCLUSIONS

This paper demonstrated that a simple linear model appears to be sufficient to decouple the forces and torques on a low-cost three-axis force sensor, under the assumption that the moment arm (point of force application) is known. This assumption may be valid for some applications, such as cooperative control or force control for surface probing. One limitation, however, is that relatively small weights were used (to provide up to 10 N of force), with relatively short moment arms (no more than 15 cm in each direction), so it is possible that nonlinearities could be observed with higher applied forces and torques. In addition, testing was performed with the OptoForce OMD-45-FE-1000N sensor, which is one of the stiffer sensors provided by the company. It is possible that the linear calibration model may not be valid for sensors with higher compliance. Furthermore, while the OMD-45-FE-1000N is stiffer than many other OptoForce sensors, it is still more compliant than a typical force sensor. This may be a disadvantage in applications where robot end-effector compliance should be minimized; for example, to preserve end-point accuracy.

We performed static tests, with applied weights, and dynamic tests, comparing to an accurate force/torque sensor, to demon-

strate that the calibrated three-axis sensor provides reasonably accurate measurements of forces applied at different (known) points with respect to the sensor origin. Static testing demonstrated that the calibrated OptoForce sensor provides measurement errors that are within 5% of the applied force. This level of performance is suitable for many robotic applications. Dynamic testing indicated that the OptoForce measurements are within 1 N of measurements from a reference 6 DOF force/torque sensor, even though differences in the time axis can significantly affect the comparison; these time differences can be caused by several factors, such as synchronization differences in reading the sensors and internal filtering (e.g., analog filters on the NI-DAQ board). Robot force control experiments, with a UR3 robot holding a passive arm and ultrasound probe, showed that the RMSE between the OptoForce sensor and the reference 6 DOF sensor is about 5% of the desired force. Component-based implementations (in C++) of the software interface to this sensor and to the UR robot are available open source.

REFERENCES

[1] P. Kazanzides, J. Zuhars, B. Mittelstadt, and R. Taylor, "Force sensing and control for a surgical robot," in *IEEE Intl. Conf. on Robotics and Automation (ICRA)*, Nice, France, May 1992, pp. 612–617.

[2] H. T. Sen, A. Cheng, K. Ding, E. Boctor, J. Wong, I. Iordachita, and P. Kazanzides, "Cooperative control with ultrasound guidance for radiation therapy," *Frontiers in Robotics and AI*, vol. 3, pp. 49,1–12, Aug 2016.

[3] H. T. Sen, M. A. L. Bell, Y. Zhang, K. Ding, E. Boctor, J. Wong, I. Iordachita, and P. Kazanzides, "System integration and in-vivo testing of a robot for ultrasound guidance and monitoring during radiotherapy," *IEEE Trans. on Biomed. Eng.*, vol. 64, no. 7, pp. 1608–1618, July 2017.

[4] M. A. L. Bell, S. Kumar, L. Kuo, H. T. Sen, I. Iordachita, and P. Kazanzides, "Toward standardized acoustic radiation force (ARF)-based ultrasound elasticity measurements with robotic force control," *IEEE Trans. on Biomed. Eng.*, vol. 63, no. 7, pp. 1517–1524, July 2016.

[5] *OMD-45-FE-1000N-DATASHEET-1.4*, OptoForce Ltd., Apr 2016.

[6] B. Vagvolgyi, S. DiMaio, A. Deguet, P. Kazanzides, R. Kumar, C. Hasser, and R. Taylor, "The Surgical Assistant Workstation: a software framework for telesurgical robotics research," in *MICCAI Workshop on Systems and Arch. for Computer Assisted Interventions*, Midas Journal: http://hdl.handle.net/10380/1466, Sep 2008.

[7] A. Deguet, R. Kumar, R. Taylor, and P. Kazanzides, "The *cisst* libraries for computer assisted intervention systems," in *MICCAI Workshop on Systems and Arch. for Computer Assisted Interventions*, Midas Journal: http://hdl.handle.net/10380/1465, Sep 2008.

[8] M. Quigley, K. Conley, B. Gerkey, J. Faust, T. B. Foote, J. Leibs, R. Wheeler, and A. Y. Ng, "ROS: an open-source Robot Operating System," in *ICRA Workshop on Open Source Software*, 2009.

[9] P. J. Berkelman, L. L. Whitcomb, R. H. Taylor, and P. Jensen, "A miniature instrument tip force sensor for robot/human cooperative microsurgical manipulation with enhanced force feedback," in *Proc. 3rd Intl Conf on Medical Image Computing and Computer-Assisted Intervention (MICCAI)*, Pittsburgh, PA, Oct 2000, pp. 897–906.

[10] B. Huang, "A flexible tactile sensor calibration method based on an air-bearing six-dimensional force measurement platform," *Review of Scientific Instruments*, vol. 86, no. 7, 2015.

[11] G. S. Faber, C.-C. Chang, I. Kingma, H. M. Schepers, S. Herber, P. H. Veltink, and J. T. Dennerlein, "A force plate based method for the calibration of force/torque sensors," *Journal of Biomechanics*, vol. 45, no. 7, pp. 1332–1338, 2012.

[12] R. Y. Tsai and R. K. Lenz, "Real time versatile robotics hand/eye calibration using 3D machine vision," in *IEEE Intl. Conf. on Robotics and Automation (ICRA)*, 1988, pp. 554–561.